

Effect of operating temperature and film thickness on the pyroelectric response of ferroelectric materials

A. Sharma, Z.-G. Ban, and S. P. Alpay^{a)}

Department of Metallurgy and Materials Engineering and Institute of Materials Science, University of Connecticut, Storrs, Connecticut 06269

J. V. Mantese

Delphi Research Laboratories, Shelby Township, Michigan 48315

(Received 8 January 2004; accepted 21 April 2004; published online 28 May 2004)

The influence of the operating temperature and film thickness on the pyroelectric properties of (001) $\text{Ba}_{0.6}\text{Sr}_{0.4}\text{TiO}_3$ (BST 60/40) epitaxial films on (001) LaAlO_3 , MgO , and Si substrates is investigated theoretically via a thermodynamic model. The results are presented using contour maps that can be used to identify “design windows” for film thickness and operating temperature for optimum pyroelectric response. For BST 60/40 on LAO and MgO large pyroelectric coefficients ($\sim 0.7 \mu\text{C cm}^{-2} \text{K}^{-1}$) are observed at near room temperature for moderate film thickness (50–200 nm). The pyroresponse of films on Si is suppressed by two orders of magnitude compared to bulk BST 60/40 due to internal stresses. Significant recovery in the pyroelectric coefficient on Si is expected for lower growth temperatures due to the reduction of thermal stresses. © 2004 American Institute of Physics. [DOI: 10.1063/1.1762691]

The pyroelectric properties of ferroelectric (FE) thin films have long been studied for applications in IR detection, most particularly, as the active sensing elements of focal plane arrays in thermal imaging systems. For these applications, electronic charge or current is generated from a FE capacitor (pixel) element in response to a temperature change relative to a reference temperature. It is preferable that FE films be integrated on-chip with the silicon readout elements so as to form a two-dimensional hybrid array in which the pixel elements are scanned electronically by IC readout elements.¹

The pyroelectric response of FE materials in thin film form, however, is significantly inferior to those of bulk single-crystal FEs due to the presence of internal stresses. Our preliminary studies have shown that internal stresses have a pronounced effect on the pyroelectric response of FE thin films and there may be orders of magnitude variation in its value.² It has been further shown that for epitaxial thin films the pyroelectric coefficient can be tuned by varying the misfit strain² which can be controlled through the selection of a substrate material and/or by varying the film thickness.³ Typically, an enhancement is expected at a critical misfit strain corresponding to the paraelectric (PE) \leftrightarrow FE phase transition.

In this letter, the effects of the film thickness and operating temperature on the pyroelectric coefficients of epitaxial FE thin films is investigated using the theoretical approach developed previously^{2,4–6} taking into account epitaxial stresses, the self-strain of the PE \leftrightarrow FE phase transformation, and the thermal stresses due to the thermal expansion mismatch between the film and the substrate. The pyroelectric response is calculated as functions of the operating temperature and film thickness and the results are presented contour

maps for $\text{Ba}_{0.6}\text{Sr}_{0.4}\text{TiO}_3$ (BST 60/40) on Si , MgO , and LaAlO_3 substrates. BST 60/40 is chosen because its PE \leftrightarrow FE transition ($\sim 2^\circ\text{C}$) is close to room temperature (RT, 25°C).

Consider an epitaxial (001) FE thin film deposited in the cubic PE state on a thick (001) cubic substrate. The thermodynamic potential \tilde{G} can be expressed in terms of the polarization P_i , the applied field E_i , and the misfit strain $u_m = (a_S - a_0)/a_S$, as^{2,5,7}

$$\begin{aligned} \tilde{G} = & a_1^*(P_1^2 + P_2^2) + a_3^*P_3^2 + a_{11}^*(P_1^4 + P_2^4) + a_{33}^*P_3^4 \\ & + a_{13}^*(P_1^2P_3^2 + P_2^2P_3^2) + a_{12}^*P_1^2P_2^2 + a_{111}(P_1^6 + P_2^6 + P_3^6) \\ & + a_{112}[(P_1^4(P_2^2 + P_3^2) + P_3^4(P_1^2 + P_2^2) + P_2^4(P_1^2 + P_3^2))] \\ & + a_{123}P_1^2P_2^2P_3^2 + \frac{u_m^2}{S_{11} + S_{12}} - (E_1P_1 + E_2P_2 + E_3P_3). \quad (1) \end{aligned}$$

a_S is the substrate lattice parameter and a_0 is the equivalent cubic cell constant of the free standing film. We define a Cartesian coordinate system with $x_1//[100]$, $x_2//[010]$, and $x_3//[001]$. The renormalized expansion coefficients of the free energy functional are:

$$\begin{aligned} a_1^* = & a_1 - u_m \frac{Q_{11} + Q_{12}}{S_{11} + S_{12}}, \quad a_3^* = a_1 - u_m \frac{2Q_{12}}{S_{11} + S_{12}}, \\ a_{11}^* = & a_{11} + \frac{1}{2} \frac{1}{S_{11}^2 - S_{12}^2} \\ & \times [(Q_{11}^2 + Q_{12}^2)S_{11} - 2Q_{11}Q_{12}S_{12}], \\ a_{33}^* = & a_{11} + \frac{Q_{12}^2}{S_{11} + S_{12}}, \quad (2) \end{aligned}$$

^{a)}Author to whom correspondence should be addressed; electronic mail: p.alpay@ims.uconn.edu

$$a_{12}^* = a_{12} - \frac{1}{S_{11}^2 - S_{12}^2} \times [(Q_{11}^2 + Q_{12}^2)S_{12} - 2Q_{11}Q_{12}S_{11}] + \frac{Q_{44}^2}{2S_{44}},$$

$$a_{13}^* = a_{12} + \frac{Q_{12}(Q_{11} + Q_{12})}{S_{11} + S_{12}},$$

where a_1 is the dielectric stiffness, a_{ij} and a_{ijk} are higher order stiffness coefficients at constant stress, Q_{ij} are the electrostrictive coefficients, and S_{ij} the elastic compliances of the film. Tensor quantities are given in the Voigt matrix notation. The temperature dependence of the dielectric stiffness a_1 is given by the Curie–Weiss law, $a_1 = (T - T_C)/2\epsilon_0 C$, where C is the Curie–Weiss constant of a bulk FE, and ϵ_0 is the permittivity of free space. The mechanical boundary conditions imposed by the epitaxy condition result in the formation of six different phases.⁴ The stable phases for epitaxial BST 60/40 films are the *paraelectric* phase ($P_1 = P_2 = P_3 = 0$), the *c* phase ($P_1 = P_2 = 0, P_3 \neq 0$), *aa* phase ($P_1 = P_2 \neq 0, P_3 = 0$), and the *r* phase ($P_1 = P_2 \neq 0, P_3 \neq 0$).

The pyroelectric coefficient p along [001] can be expressed in terms of the applied electric field $E = E_3$, the out-of-plane spontaneous polarization P_S , the out-of-plane dielectric response ϵ , and the operating temperature T as

$$p = \frac{\partial P_S}{\partial T} + E \frac{\partial \epsilon}{\partial T}. \quad (3)$$

P_S is given by the minimization of Eq. (1) with respect to the out-of-plane polarization $P_3 = P_S$:⁸

$$c \text{ phase: } P_S = \sqrt{-a_3^*/2a_{33}^*}, \quad (4)$$

$$r \text{ phase: } P_S = \sqrt{\frac{2a_{13}^*a_1^* - 2a_{11}^*a_3^* - a_{12}^*a_3^*}{4a_{11}^*a_{33}^* + 2a_{12}^*a_{33}^* - 2a_{13}^{*2}}}, \quad (5)$$

$$aa \text{ phase and paraelectric phase: } P_S = 0. \quad (6)$$

The dielectric coefficient as a function of the applied field E_3 is

$$\epsilon(E_3) = \left(\frac{\partial^2 \tilde{G}}{\partial P_3^2} \right)^{-1} = \frac{1}{2[a_3^* + a_{13}^*(P_1^2 + P_2^2) + 6a_{33}^*P_3^2]}, \quad (7)$$

where P_i are given by the equations of the state, $\partial \tilde{G} / \partial P_i = 0$ [Eqs. (4)–(6)].

The theoretical analysis is carried out for epitaxial (001) BST 60/40 on (001) Si, MgO, and LaAlO₃ with RT lattice parameters 0.5431, 0.4211, and 0.3787 nm, respectively, at $T_G = 800$ °C. When compared to the RT lattice parameter of BST 60/40 (0.3960 nm), these substrates result in a wide spectrum of internal stress states. For pseudomorphic films, Si and MgO should induce in-plane tensile stresses whereas LaAlO₃ gives rise to in-plane compressive stresses in BST 60/40. Assuming Matthews–Blakeslee type relaxation by misfit dislocations,^{5,9} the critical film thickness for misfit dislocation generation in the BST 60/40 layer at the film growth temperature $T_G = 800$ °C is found to be 1, 1.5, and 2.6 nm, respectively, for Si, MgO, and LaAlO₃ substrates, respectively.

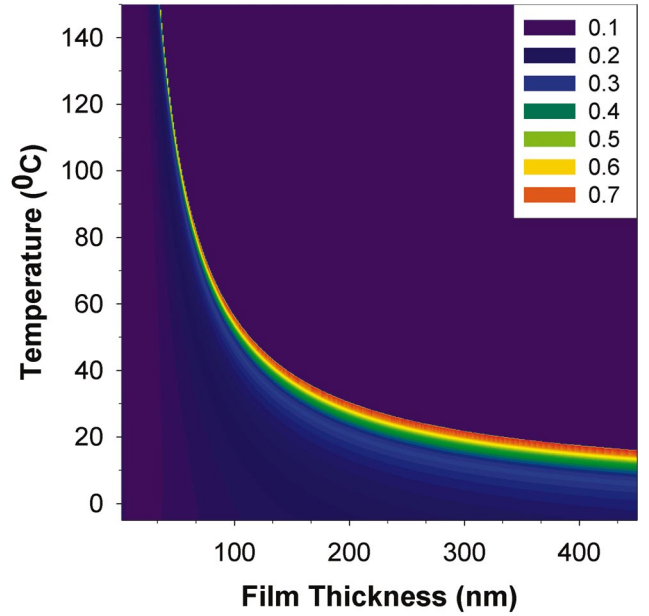


FIG. 1. (Color) Pyroelectric coefficient (in $\mu\text{C cm}^{-2} \text{K}^{-1}$) as a function of film thickness and operating temperature for (001) BST 60/40 film on (001) LaAlO₃.

Since the pyroresponse reaches a maximum near the phase transformation temperature, it is worthwhile to estimate the change in T_C as a function of the misfit strain. The variation in T_C with u_m follows from $a_3^* = 0$ and is given by

$$\Delta T_C = 4\epsilon_0 C \frac{Q_{12}}{S_{11} + S_{12}} u_m. \quad (8)$$

Compressive in-plane strains should increase the transition temperature ($\Delta T_C > 0$ since both $u_m < 0$ and $Q_{12} < 0$) and tensile in-plane strains should result in lowering of the transformation temperature and thus stabilizing the PE phase. The in-plane strain is reduced via misfit dislocation formation at T_G and the extent of the relaxation depends on the film thickness h as well as T_G . ΔT_C is, therefore, function of u_m which itself is a function of h and T_G . With increasing film thickness, it is expected that the magnitude of ΔT_C should decrease.

Figures 1–3 plot the calculated absolute values of pyroelectric coefficient as a function of the film thickness and operating temperature for BST 60/40 films on LaAlO₃, MgO, and Si substrates, respectively.¹⁰ For films on LaAlO₃ and MgO substrates, a maximum pyroresponse of $\sim 0.7 \mu\text{C cm}^{-2} \text{K}^{-1}$ is to be expected near T_C . Internal stresses due to lattice mismatch are relaxed by increasing film thickness and thus $\Delta T_C \rightarrow 0$ and a maximum pyroresponse in relatively thicker films can be obtained in the vicinity of the unconstrained single-crystal BST 60/40 FE transformation temperature. For relatively thin films (~ 10 – 70 nm) on LaAlO₃ (Fig. 1), the maximum pyroresponse is predicted at temperatures higher than 100 °C. Due to high internal stress in this thickness regime, small variations in the film thickness or temperature may shift T_C drastically and thus significantly reduce the pyroelectric coefficient. With an increase in the film thickness, the region of maximum pyroresponse broadens and shifts to lower temperatures thus providing a

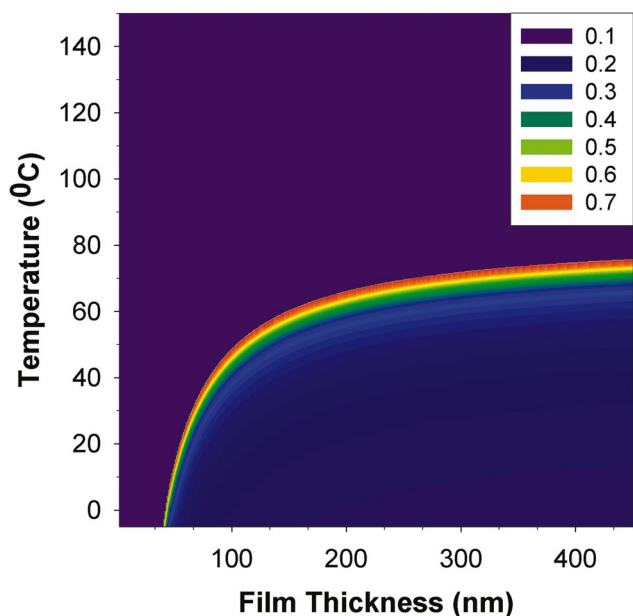


FIG. 2. (Color) Pyroelectric coefficient (in $\mu\text{C cm}^{-2} \text{K}^{-1}$) as a function of film thickness and operating temperature for (001) BST 60/40 film on (001) MgO.

wider “design window” for processing ferroelectric IR devices.

Due to the large magnitude of tensile lattice and thermal mismatch, the $\text{PE} \leftrightarrow c$ -phase transition of BST 60/40 films on Si (Fig. 3) occurs at extremely low temperatures. In the investigated thickness and temperature range, BST 60/40 is PE and the rather low pyroelectric response is due to the variation in the electric field induced polarization with temperature.² Approximately a fivefold improvement is expected in the pyroresponse when the deposition temperature is decreased from 800 °C (Fig. 3) to 500 °C (Fig. 4) due to the reduction in the thermal stresses arising from the TEC mismatch between the film and the substrate.

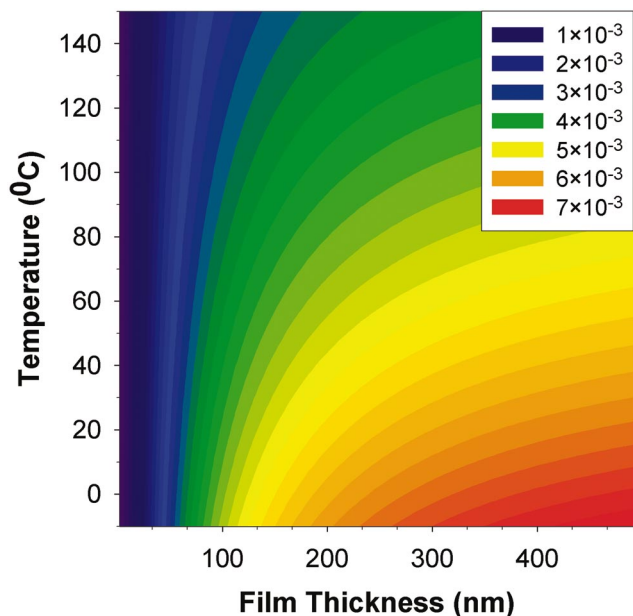


FIG. 3. (Color) Pyroelectric coefficient (in $\mu\text{C cm}^{-2} \text{K}^{-1}$) as a function of film thickness and operating temperature for (001) BST 60/40 film on (001) Si, $T_G=800$ °C.

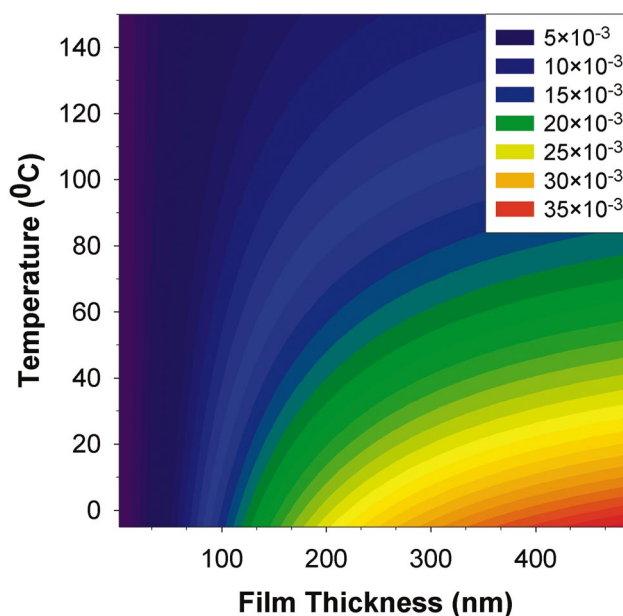


FIG. 4. (Color) Pyroelectric coefficient (in $\mu\text{C cm}^{-2} \text{K}^{-1}$) as a function of film thickness and operating temperature for (001) BST 60/40 film on (001) Si, $T_G=500$ °C.

The overwhelming majority of experimental results reported in the literature are for polycrystalline BST films on Pt coated Si substrates yielding pyroelectric coefficients in the range of 0.01–0.04 $\mu\text{C cm}^{-2} \text{K}^{-1}$.^{11,12} However, even these modest values were obtained for ferroelectric materials operated above the Curie temperature in the bolometric mode in the presence of small bias fields to yield field-induced polarization in the paraelectric state of the material. To minimize noise in an actual focal plane array; however, one must usually apply substantial bias, greatly decreasing the pyroelectric coefficient.¹³ There has been, to our knowledge, no significant pyroelectric response from ferroelectric thin films operated below the Curie temperature; as the spontaneous polarization and its change with temperature is often much less than even 0.01 $\mu\text{C cm}^{-2} \text{K}^{-1}$ in such circumstances.

This work was supported by the National Science Foundation (NSF) under Grant No. DMR-0132918.

¹R. W. Whatmore, Q. Zhang, Z. Huang, and R. A. Dorey, *Mater. Sci. Semicond. Process.* **5**, 65 (2003).
²Z.-G. Ban and S. P. Alpay, *Appl. Phys. Lett.* **82**, 3499 (2003).
³C. L. Canedy, H. Li, S. P. Alpay, L. Salamanca-Riba, A. L. Roytburd, and R. Ramesh, *Appl. Phys. Lett.* **77**, 1695 (2000).
⁴N. A. Pertsev, A. G. Zembilgotov, and A. K. Tagantsev, *Phys. Rev. Lett.* **80**, 1988 (1998).
⁵Z.-G. Ban and S. P. Alpay, *J. Appl. Phys.* **91**, 9288 (2002).
⁶A. Sharma, Z. G. Ban, S. P. Alpay, and J. V. Mantese, *J. Appl. Phys.* **95**, 3618 (2004).
⁷Z.-G. Ban and S. P. Alpay, *J. Appl. Phys.* **93**, 504 (2003).
⁸A. Amin, *J. Electroceram.* **8**, 99 (2002).
⁹J. W. Matthews and A. E. Blakeslee, *J. Cryst. Growth* **27**, 118 (1974).
¹⁰The parameters used for the calculation of Figs. 1–4 (in SI units, T in °C): $a_1^* = 4.63 \times 10^5(T - 5) - 1.90 \times 10^{10}u_m$, $a_3^* = 4.63 \times 10^5(T - 5) + 1.96 \times 10^{10}u_m$, $a_{11}^* = 2.16T \times 10^6 + 1.44 \times 10^9$, $a_{33}^* = 2.16T \times 10^6 + 7.95 \times 10^8$, $a_{12}^* = 1.73 \times 10^8$, $a_{13}^* = 1.51 \times 10^8$; data compiled from Refs. 5 and 7.
¹¹J. G. Cheng, X. J. Meng, J. Tang, S. L. Guo, and J. H. Chu, *Appl. Phys. Lett.* **75**, 3402 (1999).
¹²J.-G. Cheng, J. Tang, J.-H. Chu, and A.-J. Zhang, *Appl. Phys. Lett.* **77**, 1035 (2000).
¹³R. W. Whatmore, *Rep. Prog. Phys.* **49**, 1335 (1986).